

# Rearrangement through Berry Pseudorotation and Olefin Insertion of $d^8$ Five-Coordinate $Rh(H)(C_2H_4)(CO)_2(PH_3)$ . An ab Initio MO Study

Nobuaki Koga, Su Qian Jin,<sup>1</sup> and Keiji Morokuma\*

Contribution from the Institute for Molecular Science, Myodaiji, Okazaki 444, Japan.  
Received September 15, 1987

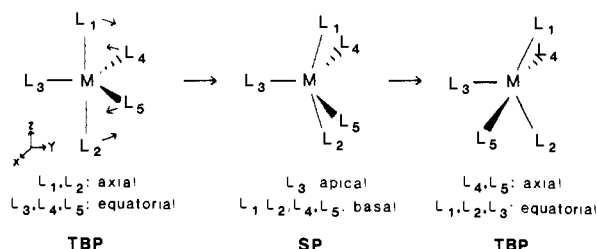
**Abstract:** The potential energy surface for intramolecular rearrangement and olefin insertion of  $Rh(H)(C_2H_4)(CO)_2(PH_3)$  (**1**) has been studied by means of an ab initio MO method. All the equilibrium structures of **1** are "trigonal bipyramidal". The relative stability of such "trigonal-bipyramidal" structures has shown the site preference of axial H and equatorial ethylene. The "square-pyramidal" structures are transition states for intramolecular rearrangement between trigonal-bipyramidal equilibrium structures through the Berry pseudorotation, with a very small intrinsic activation barrier. The potential energy surface for olefin coordination to  $Rh(H)(CO)_2(PH_3)$  to give **1** has been investigated as well. The transition states for olefin insertion are early and "square pyramidal" with basal ethylene and basal hydride, in which Rh-H is parallel to the C=C bond. The most important origin of the activation barrier (20–21 kcal/mol at the RHF level) is ascribed to the skeletal deformation from a "trigonal bipyramid" to a "square pyramid".

It is well-known that the structure of five-coordinate molecules is "nonrigid" and that rearrangements take place very easily.<sup>2</sup> Several mechanisms have been proposed for this intramolecular rearrangement,<sup>3</sup> most of which have been ruled out experimentally.<sup>4</sup> The most feasible mechanisms are Berry pseudorotation (BPR, Scheme I) and turnstile rotation mechanism (TR), although it is difficult to distinguish between them experimentally.

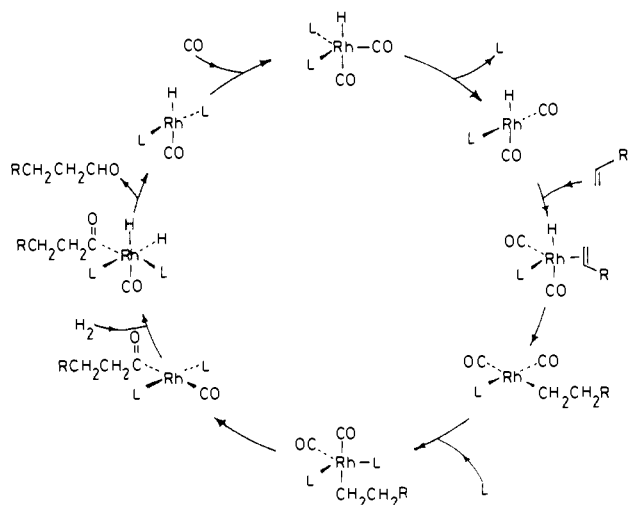
The intramolecular rearrangement of phosphoranes has been studied theoretically. Extended Hückel calculations on  $PH_5$  and  $PF_5$  reveal that the BPR process is much easier than the TR mechanism.<sup>5</sup> The activation barrier for BPR is calculated to be 2 and 1 kcal/mol for  $PH_5$  and  $PF_5$ , respectively. The preference of BPR has also been found in ab initio MO calculations. Restricted Hartree-Fock (RHF) calculations on  $PH_5$  with the 4-31G basis set have given the activation barrier of 2 and 10 kcal/mol for BPR and TR, respectively.<sup>6</sup> Similar results have been obtained by the MRDCI calculation (only one configuration was dominant and thus a single-reference SDCI was carried out) with a larger basis set: the activation barriers for BPR and TR have been calculated to be 1 and 8 kcal/mol, respectively.<sup>7</sup> As to  $PF_5$ , the activation barrier for BPR and TR has been calculated to be 5 and 18 kcal/mol, respectively, by the RHF method with the double- $\zeta$  plus polarization basis set.<sup>8</sup> Various substituted phosphoranes have also been investigated.<sup>8</sup> All the calculations have proved that for phosphorane the BPR mechanism is an easy process with a very small activation barrier.

Concerned with transition-metal complexes, the Berry pseudorotation of  $Fe(CO)_5$  and  $Fe(CO)_4(C_2H_4)$  has been calculated at the ab initio RHF level.<sup>9</sup> The activation barrier for the former is less than 1 kcal/mol and that for the latter is 13 kcal/mol. Experimentally, the activation barriers for rearrangements of

Scheme I. Berry Pseudorotation Path



Scheme II. Catalytic Cycle for Hydroformylation by a Rh Complex  $Rh(H)(CO)_2(L)$



$Fe(CO)_5$  and  $Fe(CO)_4(olef)$  have been estimated to be 1 and 11–15 kcal/mol, respectively.<sup>10,11</sup> The BPR is apparently an easy process in transition-metal complexes as well. A three-site exchange, which may be considered to be a consecutive double TR, has also been reported for  $Fe(CO)_4(olef)$ .<sup>12</sup>

There are a few well-known examples of organometallic reactions which involve as a key step the BPR rearrangement, for

(10) Spiess, H. W.; Grosescu, R.; Haebleren, U. *Chem. Phys.* **1974**, *6*, 226.

(11) (a) Kruczynski, L.; Lishing, Man, L. K. K.; Takats, J. *J. Am. Chem. Soc.* **1974**, *96*, 4006. (b) Wilson, S. T.; Coville, N. J.; Shapley, J. R.; Osborn, J. A. *J. Am. Chem. Soc.* **1974**, *96*, 4038.

(12) Cosandey, M.; von Buren, M.; Hansen, H.-J. *Helv. Chim. Acta* **1983**, *66*, 1.

(1) Permanent Address: Department of Chemistry, Beijing Normal University, Beijing, China

(2) (a) Ugi, I.; Marquarding, D.; Klusacek, H.; Gillespie, P. *Acc. Chem. Res.* **1971**, *4*, 288. (b) Holmes, R. R. *Acc. Chem. Res.* **1972**, *5*, 296.

(3) (a) Berry, R. S. *J. Chem. Phys.* **1960**, *32*, 933. (b) Muetterties, E. L. *J. Am. Chem. Soc.* **1969**, *91*, 1636. (c) Muetterties, E. L. *J. Am. Chem. Soc.* **1969**, *91*, 4115. (d) Ugi, I.; Ramirez, F.; Marquarding, D.; Klusacek, H.; Gokel, G.; Gillespie, P. *Angew. Chem., Int. Ed. Engl.* **1970**, *9*, 725.

(4) Whitesides, G. M.; Mitchell, H. G. *J. Am. Chem. Soc.* **1969**, *91*, 5384.

(5) Hoffmann, R.; Howell, J. M.; Muetterties, E. J. *J. Am. Chem. Soc.* **1972**, *94*, 3047.

(6) Altmann, J. A.; Yates, K.; Csizmadia, I. G. *J. Am. Chem. Soc.* **1976**, *98*, 1450.

(7) Shih, S.-K.; Peyerimhoff, S. D.; Buenker, R. J. *J. Chem. Soc., Faraday Trans.* **1979**, *75*, 379.

(8) (a) Strich, A.; Veillard, A. *J. Am. Chem. Soc.* **1973**, *95*, 5574. (b) Strich, A. *Inorg. Chem.* **1978**, *4*, 942.

(9) Demuyneck, J.; Strich, A.; Veillard, A. *Nouv. J. Chim.* **1977**, *1*, 217.

instance, ligand substitution reaction and cis-trans isomerization of a square-planar complex promoted by an additional ligand.<sup>13</sup> Furthermore, the BPR has been considered to exist in various stages of catalytic cycles. One such example is the catalytic cycle for hydroformylation by a Rh complex (Scheme II) proposed by Evans, Osborn, and Wilkinson,<sup>14</sup> although the rearrangement has not been explicitly taken into account. In this catalytic cycle, olefin coordinates to Rh(H)(CO)<sub>2</sub>(L) to form d<sup>8</sup> five-coordinate intermediates, and the olefin insertion follows to give four-coordinate alkyl complexes. The BPR rearrangement would take place among various five-coordinate intermediates. Therefore, in order to investigate the mechanism of this catalytic process involving d<sup>8</sup> five-coordinate intermediates, attention has to be paid to the facility of the intramolecular rearrangement.

The olefin insertion of d<sup>8</sup> five-coordinate complexes has been studied with the semiempirical and ab initio MO methods.<sup>15-18</sup> Thorn and Hoffmann have carried out extended Hückel calculations on the BPR and the olefin insertion in the d<sup>8</sup> five-coordinate Pt complex, Pt(H)(Cl)(C<sub>2</sub>H<sub>4</sub>)(PH<sub>3</sub>)<sub>2</sub>, and they found no easy insertion pathway.<sup>15</sup> Insertion-favorable structures of both trigonal bipyramidal and square pyramidal are very high in energy.

In the last few years, we have investigated several elementary organometallic reactions with the ab initio MO method with an extensive use of the energy gradient to determine the structures and energies of transition states as well as reactants and products and to discuss factors governing the activation barriers and the heats of reaction. The reactions studied include the oxidative addition/reductive elimination,<sup>19</sup> the  $\beta$ -elimination/olefin insertion,<sup>20</sup> the carbonyl insertion reaction,<sup>21</sup> and the thermolysis of a ketene complex.<sup>22</sup>

As a combination of several elementary reactions, we have recently determined the potential energy profile of a full catalytic cycle of olefin hydrogenation by the Wilkinson catalyst.<sup>23</sup> We have determined with the ab initio MO method all the equilibrium and the transition-state structures of the model Halpern catalytic cycle using ethylene as the olefin and Rh(Cl)(PH<sub>3</sub>)<sub>2</sub> as the Wilkinson catalyst. Halpern's mechanism consists of H<sub>2</sub> oxidative addition, olefin coordination, olefin insertion, and reductive elimination.<sup>24</sup> We have found that isomerization of the intermediate alkyl hydride complex is also a key elementary step. The potential energy profile of the cycle is smooth, without excessive barriers and without too stable intermediates. The rate-determining step was found to consist of olefin insertion and isomerization of the ethyl hydride complex.

Now, we focus on the catalytic cycle of the hydroformylation shown in Scheme II. As the first step toward our goal of studying this entire catalytic cycle theoretically, in this paper we concentrate on calculating with the ab initio MO method (i) the structure of

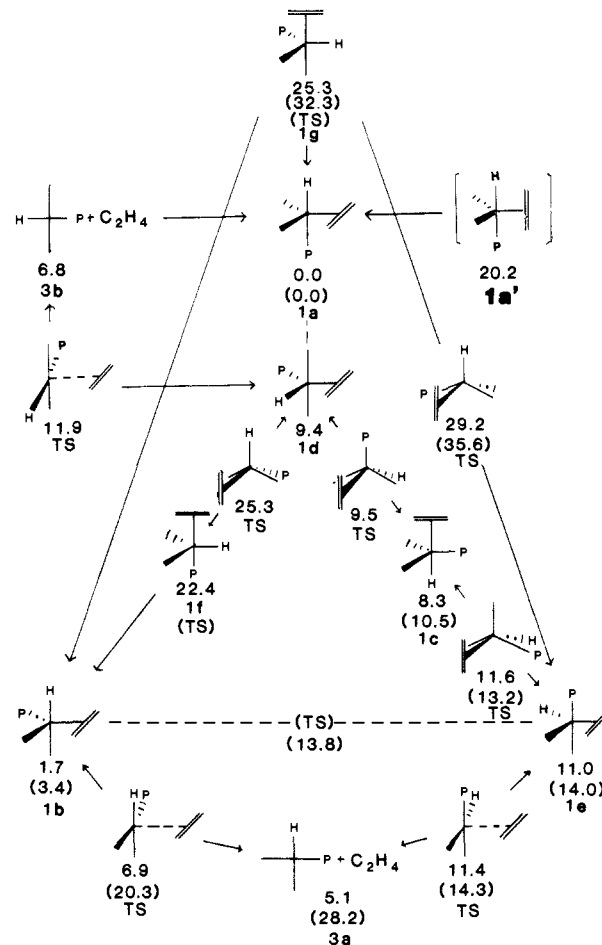


Figure 1. Potential energy profile for the olefin coordination to Rh(H)(CO)<sub>2</sub>(PH<sub>3</sub>) and the intramolecular rearrangement of Rh(H)(C<sub>2</sub>H<sub>4</sub>)(CO)<sub>2</sub>(PH<sub>3</sub>) calculated in kcal/mol at the RHF level and in parentheses at the MP2//RHF level, relative to the most stable 1a.

a d<sup>8</sup> Rh complex, Rh(H)(C<sub>2</sub>H<sub>4</sub>)(CO)<sub>2</sub>(PH<sub>3</sub>) (1), (ii) the potential energy surfaces of the rearrangement of 1, (iii) the potential surface of the ethylene coordination to Rh(H)(CO)<sub>2</sub>(PH<sub>3</sub>) (3) giving 1 (eq 1), and (iv) the potential surface of the olefin insertion from 1 (eq 2). These three steps, ethylene coordination, intramolecular rearrangement, and olefin insertion, are the model key steps involved in the catalytic cycle of olefin hydroformylation (Scheme II). We have optimized the structures of the isomers of 1 to determine the relative stability and also optimized the transition-state structures connecting them to investigate the intramolecular rearrangement. In addition, we have determined the transition states for ethylene coordination and olefin insertion. The factors that affect the relative stability of isomers and control the activation barriers for olefin insertion will be discussed.

Computational Details

All the structures of transition states as well as intermediates were optimized with the ab initio RHF method, using the GAUSSIAN82 program,<sup>25</sup> implemented with the effective core potential (ECP) code.<sup>26</sup> The basis set used is 3-21G for ethylene, CO, and hydride,<sup>27a</sup> which partici-

### Computational Details

All the structures of transition states as well as intermediates were optimized with the ab initio RHF method, using the GAUSSIAN82 program,<sup>25</sup> implemented with the effective core potential (ECP) code.<sup>26</sup> The basis set used is 3-21G for ethylene, CO, and hydride,<sup>27a</sup> which partici-

(25) Binkley, J. S.; Frisch, M. J.; DeFrees, D. J.; Raghavachari, K.; Whiteside, R. A.; Schlegel, H. B.; Pople, J. A. Carnegie-Mellon Chemistry Publishing Unit, Pittsburgh, PA, 1984.

(26) (a) McMurchie, L. E.; Davidson, E. R. *J. Comput. Phys.* **1981**, *44*, 289. (b) Martin, R. L., unpublished.

(27) (a) Binkley, J. S.; Pople, J. A.; Hehre, W. J. *J. Am. Chem. Soc.* **1980**, *102*, 939. (b) Hehre, W. J.; Stewart, R. F.; Pople, J. A. *J. Am. Chem. Soc.* **1969**, *91*, 2657.

(13) Yamamoto, A. *Organotransition Metal Chemistry*; Wiley: New York, 1986; p 199.

(14) Evans, D.; Osborn, J. A.; Wilkinson, G. *J. Chem. Soc. A* **1968**, 3133.

(15) Thorn, D. L.; Hoffmann, R. *J. Am. Chem. Soc.* **1978**, *100*, 2079.

(16) Sakaki, S.; Kato, H.; Kanai, H.; Tarama, K. *Bull. Chem. Soc. Jpn.* **1975**, *48*, 813.

(17) Grima, J. P.; Choplin, F.; Kaufmann, G. *J. Organomet. Chem.* **1977**, *129*, 221.

(18) (a) Armstrong, D. R.; Fortune, R.; Perkins, P. G. *J. Catal.* **1976**, *41*, 51. (b) Armstrong, D. R.; Novaro, O.; Ruiz-Vizcaya, M. E.; Linarte, R. *J. Catal.* **1977**, *48*, 8. (c) Daudey, J. P.; Jeung, G.; Ruiz, M. E.; Novaro, O. *Mol. Phys.* **1982**, *46*, 67.

(19) (a) Kitaura, K.; Obara, S.; Morokuma, K. *J. Am. Chem. Soc.* **1981**, *103*, 2891. (b) Obara, S.; Kitaura, K.; Morokuma, K. *Ibid.* **1984**, *106*, 7482.

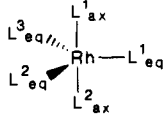
(20) (a) Koga, N.; Obara, S.; Kitaura, K.; Morokuma, K. *J. Am. Chem. Soc.* **1985**, *107*, 7109. (b) Koga, N.; Morokuma, K. *Quantum Chemistry: The Challenge of Transition Metals and Coordination Chemistry*; NATO ASI Series C, Vol. 176; Veillard, A., Ed.; Reidel: Dordrecht, 1986.

(21) (a) Koga, N.; Morokuma, K. *J. Am. Chem. Soc.* **1985**, *107*, 7230. (b) Koga, N.; Morokuma, K. *J. Am. Chem. Soc.* **1986**, *108*, 6136.

(22) Nakamura, S.; Morokuma, K. *Organometallics*, submitted for publication.

(23) Koga, N.; Daniel, C.; Han, J.; Fu, X. Y.; Morokuma, K. *J. Am. Chem. Soc.* **1987**, *109*, 3455.

(24) (a) Halpern, J.; Wong, C. S. *J. Chem. Soc., Chem. Commun.* **1973**, 629. (b) Halpern, J. In *Organotransition Metal Chemistry*; Ishii, Y., Tsutsui, M., Eds.; Plenum: New York, 1975; p 109. (c) Halpern, J.; Okamoto, T.; Zakhariyev, A. *J. Mol. Catal.* **1976**, *2*, 65.

Table I. Optimized Bond Angles of "Trigonal-Bipyramidal" Rh(H)(C<sub>2</sub>H<sub>4</sub>)(CO)<sub>2</sub>(PH<sub>3</sub>) (in deg)


	L <sup>m</sup> <sub>ax</sub> , m =		L <sup>n</sup> <sub>eq</sub> , n =			L <sup>1</sup> <sub>ax</sub> -Rh-L <sup>2</sup> <sub>ax</sub>	L <sup>n</sup> <sub>eq</sub> -Rh-L <sup>n'</sup> <sub>eq</sub> , (n, n') =			L <sup>1</sup> <sub>ax</sub> -Rh-L <sup>n</sup> <sub>eq</sub> , n =			L <sup>2</sup> <sub>ax</sub> -Rh-L <sup>n</sup> <sub>eq</sub> , n =		
	1	2	1	2	3		(1,2)	(2,3)	(3,1)	1	2	3	1	2	3
<b>1a</b>	H	PH <sub>3</sub>	C <sub>2</sub> H <sub>4</sub>	CO	CO	178.6	119.8	117.8	119.8	85.6	84.1	84.1	93.1	96.6	96.6
<b>1b</b>	H	CO	C <sub>2</sub> H <sub>4</sub>	PH <sub>3</sub>	CO	176.9	120.4	110.2	125.5	84.8	82.2	83.0	92.6	97.6	99.9
<b>1c</b>	C <sub>2</sub> H <sub>4</sub>	H	PH <sub>3</sub>	CO	CO	172.7	109.8	135.3	109.8	104.0	94.9	94.9	83.3	82.5	82.5
<b>1d</b>	CO	CO	C <sub>2</sub> H <sub>4</sub>	H	PH <sub>3</sub>	159.6	141.5	97.3	121.2	92.4	82.0	97.2	92.4	82.0	97.2
<b>1e</b>	PH <sub>3</sub>	CO	C <sub>2</sub> H <sub>4</sub>	H	CO	163.8	128.9	105.3	125.7	91.4	83.7	93.0	92.3	81.7	97.6
<b>1f</b>	C <sub>2</sub> H <sub>4</sub>	PH <sub>3</sub>	H	CO	CO	159.5	115.1	129.6	115.1	80.6	95.4	95.4	79.0	93.3	93.3
<b>1g</b>	C <sub>2</sub> H <sub>4</sub>	CO	H	PH <sub>3</sub>	CO	157.6	124.5	116.4	119.0	80.9	99.1	93.6	76.7	93.7	97.0

pate in the hydroformylation catalytic cycle. The STO-2G set is used for the "spectator" ligand, PH<sub>3</sub>.<sup>27b</sup> For RH, the relativistic effective core potential and valence (4d, 5s, 5p) double- $\zeta$  basis functions determined by Hay and Wadt were adopted.<sup>28</sup>

In carrying out the geometry optimization, the standard value of threshold for the maximum energy gradient ( $4.5 \times 10^{-4}$ ) has been used except for the internal rotation of PH<sub>3</sub> around the Rh-P bond. PH<sub>3</sub> rotates around the Rh-P bond almost freely. Therefore, the complete optimization with respect to this degree of freedom requires many optimization cycles. In order to save computational time, the energy gradient threshold for this rotation was set to be  $1 \times 10^{-3}$ . In most geometry optimizations, however, the energy gradient with respect to this rotation at the optimized structures were less than  $4.5 \times 10^{-4}$ , except for **1d**, **2a**, the transition state between **1d** and **1g**, and the transition states for olefin insertion from **1b**.

We also carried out the frozen-core second-order Møller-Plesset perturbation calculation (MP2) at the RHF optimized geometries (correlating for instance 50 valence electrons in **1**) to investigate the effect of electron correlation. The electron correlation often makes a metal-ethylene bond stronger and a transition state more stable.

#### Potential Surface for Intramolecular Rearrangement of Rh(H)(C<sub>2</sub>H<sub>4</sub>)(CO)<sub>2</sub>(PH<sub>3</sub>) (**1**) and Olefin Coordination to Rh(H)(CO)<sub>2</sub>(PH<sub>3</sub>) (**3**)

In Figure 1 is shown the overall potential energy surface for rearrangement of **1** calculated at the RHF level. A priori, one can conceive seven "trigonal-bipyramidal" (TBP) structures as well as nine "square-pyramidal" (SP) structures interconnecting the TBP structures, provided that the enantiomers of chiral isomers are not counted. It should be noted that the required symmetry of structure **1** is lower than  $D_{3h}$  or  $C_{4v}$  and thus **1**'s are not exactly trigonal bipyramidal or square pyramidal. The geometry optimization has shown that five of the TBP structures, **1a** to **1e**, are equilibrium structures and that the other two, **1f** and **1g**, are transition states for rearrangement. The SP structures are transition states for rearrangement connecting "trigonal bipyramidal" structures through BPR. For the rearrangement between **1a** and **1d** and between **1b** and **1e**, ethylene dissociates at the transition region, as will be discussed in detail later; the rearrangement takes place via a four-coordinate complex by dissociating and reCOORDINATING ethylene. In the present section, we will first discuss the optimized structures of TBP complexes and then we will focus on the TBP or SP transition states for intramolecular rearrangement. The olefin coordination reaction will be discussed as well.

**TBP Five-Coordinate Complexes.** The optimized structures of TBP five-coordinate complexes are shown in Tables I and II. All the L<sub>ax</sub>-Rh-L<sub>eq</sub>, L<sub>eq</sub>-Rh-L<sub>eq</sub>, and L<sub>ax</sub>-Rh-L<sub>ax</sub> angles in Table I are in the vicinity of 90°, 120°, and 180°, respectively. These features of the optimized structures indicate that they are nearly trigonal bipyramidal, although we say again that they do not have a  $D_{3h}$  symmetry and are not truly TBP.

Larger deviations from the ideal TBP are as follows: (1) the small H<sub>ax</sub>-Rh-L<sub>eq</sub> angles (82–86°) in **1a**, **1b**, and **1c**, leading to the large L<sub>ax</sub>-Rh-L<sub>eq</sub> angles (93–104°) in which L<sub>ax</sub> is trans to

Table II. Optimized Bond Lengths of "Trigonal-Bipyramidal" Rh(H)(C<sub>2</sub>H<sub>4</sub>)(CO)<sub>2</sub>(PH<sub>3</sub>) (in Å)

Rh—H	
axial	1.567 ( <b>1a</b> ), 1.562 ( <b>1b</b> ), 1.542 ( <b>1c</b> )
equatorial	1.621 ( <b>1d</b> ), 1.623 ( <b>1e</b> ), 1.616 ( <b>1f</b> ), 1.615 ( <b>1g</b> )
Rh—PH <sub>3</sub>	
axial	2.374 ( <b>1a</b> ), 2.319 ( <b>1e</b> ), 2.293 ( <b>1f</b> )
equatorial	2.335 ( <b>1b</b> ), 2.356 ( <b>1c</b> ), 2.365 ( <b>1d</b> ), 2.382 ( <b>1g</b> )
Rh—CO	
axial	2.006 ( <b>1b</b> ), 1.912 ( <b>1d</b> ), 1.909 ( <b>1e</b> ), 1.820 ( <b>1g</b> )
equatorial	1.950 ( <b>1a</b> ), 1.952 ( <b>1b</b> ), 1.948 ( <b>1c</b> ), 2.011 ( <b>1e</b> ), 1.999 ( <b>1f</b> ), 2.120 ( <b>1g</b> )
Rh—C <sub>2</sub> H <sub>4</sub> <sup>a</sup>	
axial	2.307 ( <b>1c</b> ), 2.235 ( <b>1f</b> ), 2.302 ( <b>1g</b> )
equatorial	2.136 ( <b>1a</b> ), 2.106 ( <b>1b</b> ), 2.127 ( <b>1d</b> ), 2.100 ( <b>1e</b> )
C=C in ethylene	
axial	1.352 ( <b>1c</b> ), 1.365 ( <b>1f</b> ), 1.356 ( <b>1g</b> )
equatorial	1.380 ( <b>1a</b> ), 1.391 ( <b>1b</b> ), 1.396 ( <b>1d</b> ), 1.402 ( <b>1e</b> )

<sup>a</sup>Distance between Rh and the midpoint of C=C.

H<sub>ax</sub>, (2) the small H<sub>eq</sub>-Rh-L<sub>ax</sub> angles (77–84°) in **1d**, **1e**, **1f**, and **1g**, giving the small L<sub>ax</sub>-Rh-L<sub>ax</sub> angles (158–164°), (3) the large CO<sub>eq</sub>-Rh-CO<sub>eq</sub> angle of 135° in **1c**, and (4) the small angle of equatorial H-Rh-P of **1d** (97.3°) and H-Rh-CO of **1e** (105.3°). The first two features can be explained in terms of the small steric hindrance of H as shown below. A ligand can avoid a steric repulsion by bending toward the small H ligand.



The small H<sub>ax</sub>-Rh-L<sub>eq</sub> angle (81°) has been observed in the X-ray study of trigonal-bipyramidal Rh(H)(CO)(PPh<sub>3</sub>)<sub>3</sub> between the axial H and the equatorial PPh<sub>3</sub>.<sup>29</sup> The large CO<sub>eq</sub>-Rh-CO<sub>eq</sub> angle may be ascribed to the steric repulsion between carbonyl groups. The last two small angles promote the back-donation from Rh to  $\pi^*$  of ethylene, as will be discussed later.

All the axial Rh-H, Rh-P, and Rh-CO bonds shown in Table II are shorter than the corresponding equatorial bonds and thus should be stronger, except for the cases influenced by the trans H, as discussed below. These bonds prefer the axial position. The calculated axial Rh-H distance (1.562–1.567 Å) is close to the X-ray value of  $1.60 \pm 0.12$  Å.<sup>29</sup> The X-ray distances of axial Rh-CO and equatorial Rh-P have been 1.829 and 2.315–2.336 Å, respectively.<sup>29</sup> Although the calculated bond distances are slightly longer, they are in reasonable agreement with the X-ray values, considering the present level of calculation.

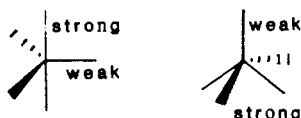
In comparing the Rh-L<sub>ax</sub> bond distances, one can find the so-called trans influence. H makes the trans Rh-L<sub>ax</sub> bond the longest (Rh-PH<sub>3</sub> bond of 2.374 Å in **1a**, Rh-CO bond of 2.006

(28) Hay, P. J.; Wadt, W. R. *J. Chem. Phys.* **1985**, *82*, 270.

(29) La Placa, S. J.; Ibers, J. A. *Acta Crystallogr.* **1965**, *18*, 511.

**Table III.** Energy Difference (in kcal/mol) between Two TBP Structures of Rh(H)(C<sub>2</sub>H<sub>4</sub>)(CO)<sub>2</sub>(PH<sub>3</sub>) Connected by Exchange of Axial and Equatorial Ligands

L <sup>1</sup>	L <sup>2</sup>	$E(L_{ax}^1, L_{eq}^2) - E(L_{eq}^1, L_{ax}^2)$
H	C <sub>2</sub> H <sub>4</sub>	-22.4 <b>1a-1f</b> -23.6 <b>1b-1g</b>
H	CO	-11.0 <b>1a-1e</b> -7.7 <b>1b-1d</b> -17.0 <b>1c-1g</b> -9.3 <b>1b-1e</b> -14.1 <b>1c-1f</b>
C <sub>2</sub> H <sub>4</sub>	CO	6.6 <b>1c-1b</b> 15.9 <b>1g-1d</b> 11.4 <b>1f-1e</b>
C <sub>2</sub> H <sub>4</sub>	PH <sub>3</sub>	8.3 <b>1c-1a</b> 14.3 <b>1g-1e</b>
CO	PH <sub>3</sub>	1.7 <b>1b-1a</b> -1.6 <b>1d-1e</b> 2.9 <b>1g-1f</b>

**Chart I.** Relative Strength of Bonds in TBP and BP Complexes

Å in **1b**, and Rh-C<sub>2</sub>H<sub>4</sub> bond of 2.307 Å in **1c**) while the Rh-L<sub>ax</sub> bonds trans to ethylene are the shortest (Rh-H bond of 1.542 Å in **1c**, Rh-PH<sub>3</sub> bond of 2.293 Å in **1f**, and Rh-CO bond of 1.820 Å in **1g**). Although the trans influences of PH<sub>3</sub> and CO are between those of H and ethylene, one may notice that CO makes the Rh-C<sub>2</sub>H<sub>4</sub> bond exceptionally long: 2.302 Å in **1g**. The back-donations to CO and ethylene share the same donor orbital, d<sub>yz</sub>, leading to the weaker Rh-C<sub>2</sub>H<sub>4</sub> bond trans to CO.

The equatorial Rh-ethylene distances are shorter than the axial ones and the C=C distance of the equatorial ethylene is longer than that of the axial ethylene, indicating that the equatorial Rh-C<sub>2</sub>H<sub>4</sub> bonding interaction is stronger than the axial. The optimized structure has ethylene coordinated in the equatorial plane. The structure in which the C=C bond in **1a** is rotated to be parallel to the Rh-H bond (**1a'**) is higher in energy than **1a** by 20.2 kcal/mol. The equatorial in-plane ethylene is much more stable than the equatorial vertical ethylene. The strong back-donation from Rh d<sub>xy</sub> to ethylene π\* and the small repulsion between ethylene and the Rh-L<sub>ax</sub> bonds in the in-plane coordination mode contribute to this preference, as will be discussed later.

The most stable isomers of **1** are **1a** and **1b** with axial H and equatorial ethylene and the most unstable ones are **1f** and **1g** with equatorial H and axial ethylene. **1c** with axial H and axial ethylene and **1d** and **1e** with equatorial H and equatorial ethylene are between the extremes. Comparison of the relative stability among the isomers of **1**, shown in Table III, provides the order of the preference of axial over equatorial: H > PH<sub>3</sub> ~ CO > C<sub>2</sub>H<sub>4</sub>. CO and PH<sub>3</sub> are similar to each other in the axial preference. These results of relative stability indicate that the site preference of axial H and equatorial ethylene governs the gross feature of relative stability of the isomers of **1**.

Rossi and Hoffmann have studied the structures of five-coordinate complexes based on the overlap and symmetry of the fragment orbitals and have deduced the relative σ M-L bond strength as shown in Chart I.<sup>30</sup> The axial M-L bond in the TBP structure is stronger than the equatorial bond. In the TBP complex the e' orbitals consisting mainly of d<sub>xy</sub> and d<sub>x<sup>2</sup>-y<sup>2</sup></sub> are occupied and the metal s and p orbitals have to play a dominant role in the M-L<sub>eq</sub> bond. On the other hand, the d<sub>z<sup>2</sup></sub> orbital is empty and thus available to M-L<sub>ax</sub> bonding, making the axial bond stronger than the equatorial bond. In particular, the d character of the metal orbital in the M-H bond is large.<sup>31</sup> Therefore, the axial Rh-H

**Table IV.** Energy Decomposition Analysis of Interaction between Rh(H)(CO)<sub>2</sub>(PH<sub>3</sub>) and Ethylene (in kcal/mol)

	<b>1a</b>	<b>1a'</b>	<b>1d</b>	<b>1f</b>
INT	-30.5	-10.2	-39.2	-32.3
ES+EX	38.9	53.2	41.3	24.6
FCTPLX	-33.0	-34.2	-35.3	-30.7
BCTPLX	-33.8	-28.4	-40.9	-21.2
residual	-2.6	-0.8	-4.4	-5.0

**Table V.** Optimized Bond Angles of "Square-Pyramidal" Transition States for Rearrangement of Rh(H)(C<sub>2</sub>H<sub>4</sub>)(CO)<sub>2</sub>(PH<sub>3</sub>) (in deg)

L <sub>ap</sub>	L <sup>m</sup> <sub>ba</sub> , m =				L <sup>n</sup> <sub>ba</sub> -Rh-L <sup>m</sup> <sub>ba</sub> , (n, m) =		
	1	2	3	4	(1, 3)	(2, 4)	
<b>1d-1c</b>	PH <sub>3</sub>	C <sub>2</sub> H <sub>4</sub>	CO	H	CO	150.0	154.8
<b>1c-1e</b>	CO	C <sub>2</sub> H <sub>4</sub>	PH <sub>3</sub>	H	CO	157.3	146.4
<b>1d-1f</b>	H	C <sub>2</sub> H <sub>4</sub>	CO	PH <sub>3</sub>	CO	177.9	154.9
<b>1e-1g</b>	H	C <sub>2</sub> H <sub>4</sub>	CO	CO	PH <sub>3</sub>	179.4	152.9

	L <sub>ap</sub> -Rh-L <sup>m</sup> <sub>ba</sub> , m =			
	1	2	3	4
<b>1d-1c</b>	116.2	99.8	93.8	99.8
<b>1c-1e</b>	110.5	99.3	92.1	109.0
<b>1d-1f</b>	97.4	102.5	84.7	102.5
<b>1e-1g</b>	93.7	112.2	86.6	94.9

bond which can use a d orbital is stronger than the equatorial Rh-H bond to which only s and p orbitals are available. As to the σ M-L bond, the present ab initio results for Rh-H, Rh-P, and Rh-CO bonds are in agreement with this overlap argument.

Contrary to this, the equatorial Rh-C<sub>2</sub>H<sub>4</sub> bond is shorter and stronger than the corresponding axial bond. In the Rh-C<sub>2</sub>H<sub>4</sub> bond, the back-donation to a π\* orbital plays a crucial role as discussed by Rossi and Hoffmann. The occupied e' orbitals are destabilized in energy by the other two equatorial ligands and are available for easy back-donation. A large hybridization of p orbitals into d orbitals stretching the orbital lobe toward C<sub>2</sub>H<sub>4</sub> also takes place. These two factors contribute to the stronger back-donation in the equatorial bond than in the axial bond. One would realize that CO also has the electron-accepting π\* orbital, as in C<sub>2</sub>H<sub>4</sub>. The Rh-CO<sub>ax</sub> bond is, however, shorter than the Rh-CO<sub>eq</sub> bond, indicating that the σ effect is dominant in the Rh-CO bond.

We have carried out the energy decomposition analysis (EDA)<sup>32</sup> to obtain evidences supporting these qualitative discussions on the Rh-C<sub>2</sub>H<sub>4</sub> bond. In the EDA, the RHF interaction energy (INT) between the Rh(H)(CO)<sub>2</sub>(PH<sub>3</sub>) and the C<sub>2</sub>H<sub>4</sub> fragment is evaluated by increasing the Rh-C<sub>2</sub>H<sub>4</sub> distance to infinity while holding the geometries at their geometries in the complex. The interaction energy is further decomposed into the sum of electrostatic and exchange interaction (ES+EX), the forward (FCTPLX) and the backward (BCTPLX) donative interaction, and the residual interaction. Omitting **1c** and **1g** (the Rh-C<sub>2</sub>H<sub>4</sub> bond is much longer) and **1b** and **1e** (nearly equivalent to **1a** and **1d**, respectively) we have carried out the EDA for **1a**, **1a'**, **1d**, and **1f** and the results are shown in Table IV.

A comparison among **1a**, **1d**, and **1f** shows that (1) the back-donative interaction (BCTPLX) is much stronger in **1a** and **1d** with an equatorial ethylene than in **1f** with an axial ethylene and that (2) the (ES+EX) in **1a** and **1d** is more repulsive than that in **1f**. The occupied e' orbitals cause both a stronger back-donation and a larger exchange repulsion between Rh and ethylene in **1a** and **1d**. These EDA results agree well with the above qualitative

(30) Rossi, A. R.; Hoffmann, R. *Inorg. Chem.* **1975**, *14*, 365.(31) Low, J. J.; Goddard, W. A. III *J. Am. Chem. Soc.* **1986**, *108*, 6115.(32) (a) Morokuma, K.; Kitaura, K. *Chemical Application of Atomic and Molecular Electrostatic Potentials*; Politzer, P., Truhler, D. G., Eds.; Plenum: New York, 1981. (b) Kitaura, K.; Sakaki, S.; Morokuma, K. *Inorg. Chem.* **1981**, *20*, 2292.

**Table VI.** Optimized Bond Lengths of "Square-Pyramidal" Transition States for Rearrangement of Rh(H)(C<sub>2</sub>H<sub>4</sub>)(CO)<sub>2</sub>(PH<sub>3</sub>) (in Å)

	Rh—H	
apical	1.657 (1d–1f), 1.659 (1e–1g)	
basal	1.604 (1d–1c), 1.579 (1c–1e)	
	Rh—PH <sub>3</sub>	
apical	2.366 (1d–1c)	
basal	2.330 (1c–1e), 2.305 (1d–1f), 2.350 (1e–1g)	
	Rh—CO	
apical	2.055 (1c–1e)	
basal	1.916 (1d–1c), 1.913 (1c–1e), 1.941 (1d–1f) 1.954 (1e–1g), 1.856 (1e–1g)	
	Rh—C <sub>2</sub> H <sub>4</sub> <sup>a</sup>	
basal	2.159 (1d–1c), 2.214 (1c–1e) 2.177 (1d–1f), 2.199 (1e–1g)	
	C=C in Ethylene	
basal	1.386 (1d–1c), 1.369 (1c–1e) 1.377 (1d–1f), 1.374 (1e–1g)	

<sup>a</sup>Distance between Rh and the midpoint of C=C.

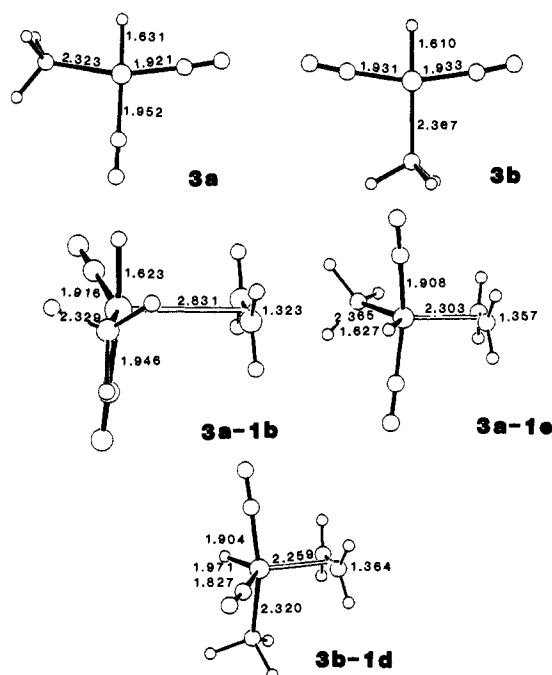
discussions. A comparison between **1a** and **1a'** indicates that **1a** is more stable than **1a'** because of a smaller exchange (and electrostatic) repulsion between the Rh fragment and ethylene, augmented with a stronger back-donative interaction.

**Rearrangement of Rh(H)(CO)<sub>2</sub>(PH<sub>3</sub>)(C<sub>2</sub>H<sub>4</sub>) via Berry Pseudorotation.** As shown in Figure 1, we have been able to find four transition states for intramolecular rearrangement, **1d–1c**, **1c–1e**, **1d–1f**, and **1e–1g**. In Tables V and VI are shown the optimized structures of the transition states determined at the RHF level. The reaction coordinate at the transition states calculated from the approximate force constant matrix shows that the reaction mechanism is just the change of angles as shown in Scheme I, corresponding to the BPR, and that no turnstile rotation is involved. In addition, the transition-state structures are geometrically located between two "TBP" isomers to be connected by BPR. Therefore, we conclude that the transition states we obtained are those for BPR, even though we have not actually followed the reaction coordinate from the transition states to the reactants and products. Though we have not searched exhaustively, we have not found any low-energy transition state for turnstile rotation or three-state exchange (double turnstile rotation).

Table V indicates that the structures of all these transition states are approximately square pyramidal in which the pivot ligand for BPR is located apical and the other four ligands are basal. The bond lengths in the SP transition states summarized in Table VI and those in the TBP equilibrium geometries in Table II show that the bond length decreases in the following order: ap > eq > ba > ax for Rh—H, Rh—PH<sub>3</sub>, and Rh—CO bonds. The apical bond is the longest and thus the weakest. One can imagine the square-pyramidal complex to be constructed by pyramidalizing the square-planar d<sup>8</sup> four-coordinate complex and adding the extra apical ligand. The overlap repulsion between d<sub>z<sup>2</sup></sub> (cf. Scheme I) and the ligand orbital takes place, making the Rh—L<sub>ap</sub> bond weaker. For Rh—ethylene, the trend is reversed completely: ax > ba > eq. No transition state with an apical C<sub>2</sub>H<sub>4</sub> has been found.

If the rearrangement process is thermoneutral, the activation barrier is intrinsically that of BPR. If it is not thermoneutral, the barrier reflects the heat of reaction as well. Paying attention to relatively thermoneutral rearrangements **1d–1c** and **1c–1e**, one finds that the barriers are very low; the barrier from **1d** to **1c** is only 0.1 kcal/mol, and that from **1e** to **1c** is 0.6 kcal/mol. One may say that the BPR in this complex is an easy process as in other systems previously studied.

**Olefin Dissociation and Coordination.** At the RHF level of calculation, we have found no transition state connecting **1a** and **1d** or **1b** and **1e**. Since the Rh—apical ethylene bond is very weak, ethylene dissociates and leaves a four-coordinate Rh(H)(CO)<sub>2</sub>(PH<sub>3</sub>), **3a** or **3b**. After the dissociation ethylene rotates 90° around the Rh—C<sub>2</sub>H<sub>4</sub> axis and associates again. We found the transition

**Figure 2.** Optimized structures of Rh(H)(CO)<sub>2</sub>(PH<sub>3</sub>) and the transition states between Rh(H)(CO)<sub>2</sub>(PH<sub>3</sub>) and Rh(H)(C<sub>2</sub>H<sub>4</sub>)(CO)<sub>2</sub>(PH<sub>3</sub>) in Å.

states for the ethylene association from **3a** to **1b** or **1e** and from **3b** to **1d**. The dissociation of C<sub>2</sub>H<sub>4</sub> to **3b** to give **1a** takes place without a barrier, probably because of its largest exothermicity of 7 kcal/mol. The optimized structures of **3** and the transition states between isomers of **3** and those of **1** are shown in Figure 2.

It is well-known, however, that a computation without electron correlation often underestimates the strength of a metal–ligand bond when both donation and back-donation are important.<sup>33</sup> In order to investigate the effect of electron correlation on the potential energy surface, we have carried out the RHF geometry optimization of BPR transition states connecting **1b** and **1e** with the Rh–ethylene distance fixed at several distances and have calculated the MP2 energies at the RHF optimized structures. The RHF potential curve decreases its energy as the Rh–ethylene distance increases, showing again that the BPR takes place upon ethylene dissociation. The MP2 curve, on the other hand, has a substantial minimum around 2.3 Å, to indicate that the transition state connecting **1b** and **1e** with a coordinated ethylene probably exists, if the electron correlation is properly taken into account.

We have also calculated the energies of **1b** and **1e** by the MP2 method at the RHF optimized geometries. The energies are shown in Figure 1. The correlation does not change the energy difference between **1b** and **1e**. This is reasonable, because in both complexes ethylene coordinates in the equatorial plane. But, the ethylene coordination energy itself changes drastically. At the RHF and MP2 level of calculations, the ethylene coordination energy for **1b** is 3.4 and 24.8 kcal/mol, respectively. The electron correlation makes the Rh–ethylene bond stronger by 20 kcal/mol. Though the transition-state RHF optimized at the Rh–ethylene distance of 2.3 Å is lower in energy than **1e**, **1e** is expected to be more stable than the transition state, if the optimization were performed at the MP2 level. In such a case, the barrier for BPR from **1e** to **1b** would be very small. We expect that the situation for the process from **1a** to **1d** is similar, though we did not carry out such calculations. The transition state for ethylene coordination has disappeared and the potential surface is down-hill at the MP2 level

(33) (a) Widmark, P.-O.; Roos, B. O.; Siegbahn, P. E. M. *J. Phys. Chem.* **1985**, *89*, 2180. (b) Lüthi, H. P.; Siegbahn, P. E. M.; Almlöf, J. *J. Phys. Chem.* **1985**, *89*, 2156. (c) Moncrieff, D.; Ford, C. P.; Hillier, I. H.; Saunders, V. R. *J. Chem. Soc., Chem. Commun.* **1983**, 1108. (d) Dedieu, A.; Sakaki, S.; Strich, A.; Siegbahn, P. E. M. *Chem. Phys. Lett.* **1987**, *133*, 317. (e) Lüthi, H. P.; Siegbahn, P. E. M.; Almlöf, J.; Faegri, K., Jr.; Heiberg, A. *Chem. Phys. Lett.* **1984**, *111*, 1. (f) Taylor, T. E.; Hall, M. B. *Ibid.* **1985**, *114*, 338.

Scheme III. Possible Paths of Intramolecular Olefin Insertion.

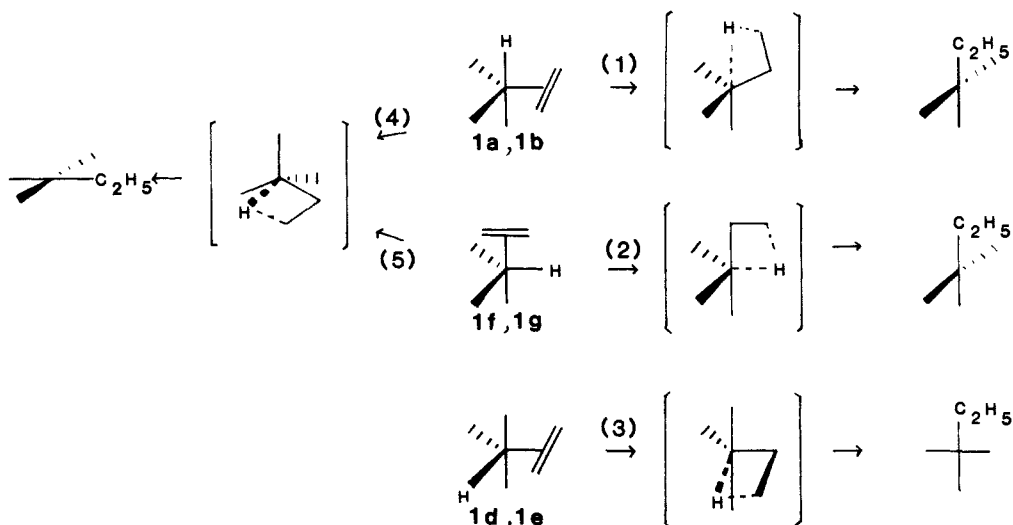
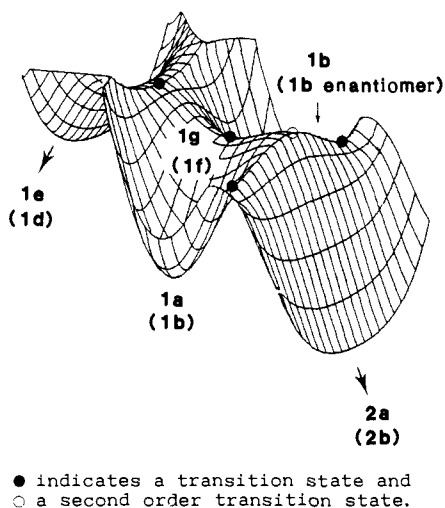


Chart II. Schematics of the Potential Profile for the Region Consisting of 1e, 1a, 1b, 1g, and 2a (The Region of 1d, 1b, 1f, 1b Enantiomer, and 2b Is Essentially the Same)



of calculation, since MP2 exothermicity of ethylene coordination at the MP2 level is larger by 20 kcal/mol than that at the RHF level.

**High-Energy Trigonal-Bipyramidal Transition States.** As we mentioned at the beginning of this section, the most unstable "trigonal-bipyramidal" isomers, **1f** and **1g**, are not equilibrium structures. The former is the transition state connecting **1b** and its enantiomer and the latter **1a** and **1b**. Though these high-energy isomers could be of little importance in the actual reaction process, we will discuss these unusual cases in detail for a pedagogical purpose. The processes connecting the transition states and the equilibrium structures are BPR. One may consider the situation as follows. The BPR from **1a** and **1b**, the most stable isomers with axial H and equatorial ethylene, to **1f** and **1g**, the least stable, is so endothermic that the transition state has collapsed to the product, **1f** and **1g**, respectively.

Although **1f** and **1g** are transition states, as was discussed before, there exist transition states connecting and located between them and the equilibrium structures, **1d** and **1d**, respectively (cf. Figure 1 and Table V). The geometries of these transition states **1f** → **1d** and **1g** → **1e** are similar to those of the BPR transition states for **1c** → **1d** and **1c** → **1e**, indicating that these rearrangements are again BPR. The qualitative feature of these complicated potential profiles can be depicted in Chart II. A force constant to the direction perpendicular to the reaction coordinate changes sign between the TS(**1d**–**1f**) and **1f** and between TS(**1e**–**1g**) and **1g**.

Table VII. Optimized Bond Angles of Transition States for Olefin Insertion of Rh(H)(C<sub>2</sub>H<sub>4</sub>)(CO)<sub>2</sub>(PH<sub>3</sub>) (in deg)

	L <sub>ap</sub>	L <sup>m</sup> <sub>ba</sub> , m =		H–Rh–L <sup>1</sup> <sub>ba</sub>	C <sub>2</sub> H <sub>4</sub> –Rh–L <sup>2</sup> <sub>ba</sub>
		1	2		
<b>1a</b> – <b>2a</b>	CO	CO	PH <sub>3</sub>	148.1	160.2
<b>1b</b> – <b>2a</b>	PH <sub>3</sub>	CO	CO	157.8	154.7
<b>1b</b> – <b>2b</b>	CO	PH <sub>3</sub>	CO	163.5	145.7
	L <sub>ap</sub> –Rh–H	L <sub>ap</sub> –Rh–CH <sub>2</sub>	L <sub>ap</sub> –Rh–L <sup>1</sup> <sub>ba</sub>	L <sub>ap</sub> –Rh–L <sup>2</sup> <sub>ba</sub>	
<b>1a</b> – <b>2a</b>	95.3	95.9	116.2	91.9	
<b>1b</b> – <b>2a</b>	93.3	95.8	107.1	105.5	
<b>1b</b> – <b>2b</b>	93.6	98.3	100.2	113.5	

### Intramolecular Olefin Insertion

For intramolecular olefin insertion of TBP ethylene hydride complexes, the five reaction paths shown in Scheme III are conceivable. In the first path, the axial hydride and the equatorial ethylene in **1a** or **1b** react by insertion of C<sub>2</sub>H<sub>4</sub> into the Rh–H bond. During the reaction ethylene has to rotate around the Rh–C<sub>2</sub>H<sub>4</sub> axis by about 90° to approach the hydride. In the second path, the axial C<sub>2</sub>H<sub>4</sub> and the equatorial H in **1f** or **1g** react by hydride migration toward olefin. In the third path, the equatorial H and the equatorial C<sub>2</sub>H<sub>4</sub> in **1d** and **1e** react within the equatorial plane. In the above three paths, the transition state would be more or less trigonal bipyramidal with two approximately "axial" ligands. In the fourth and fifth paths the reaction takes place between the basal H and the basal olefin at the square-pyramidal transition state, starting from **1a** or **1b** and **1f** or **1g**, respectively. The path to the transition state would involve the rotation of ethylene around the Rh–C<sub>2</sub>H<sub>4</sub> axis as well as the BPR. In all cases, the product will be a square-planar ethyl complex.

Therefore, we have searched in the wide range of geometry the corresponding transition-state structures. The potential energy profile of olefin insertion we have finally obtained is shown in Figure 3. All the transition-state structures for olefin insertion, whose structural details are shown in Tables VII and VIII, are "square pyramidal", in which both H and ethylene are located in the basal position to facilitate the formation of the four-centered transition states. They all come from the most stable isomers, **1a** and **1b**, with activation barriers of 20–21 kcal/mol at the RHF level. The MP2 calculation for TS(**1a**→**2a**) in Figure 4 shows that the barrier is insensitive to electron correlation.

The transition-state geometries and the approximate normal coordinates at the transition state indicate that the reaction coordinate from the reactant up to the transition state is the ethylene

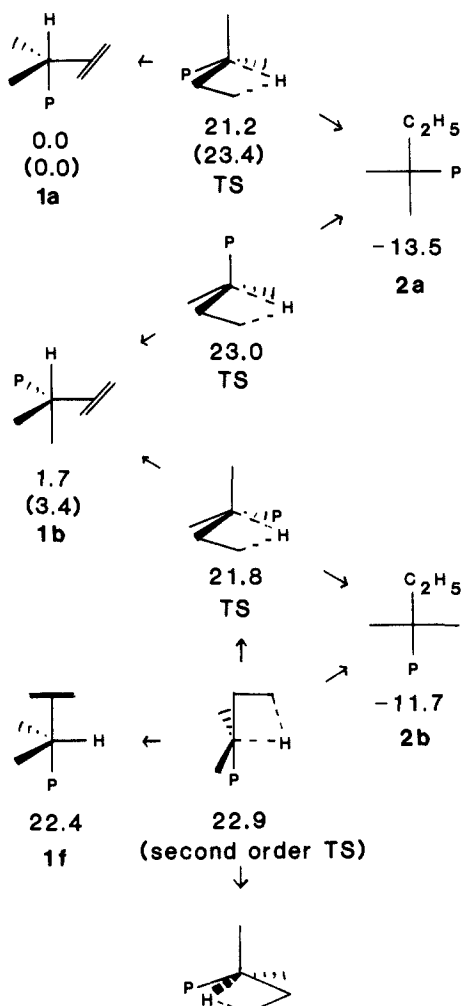


Figure 3. Potential energy profile for olefin insertion of  $\text{Rh}(\text{H})(\text{C}_2\text{H}_4)(\text{CO})_2(\text{PH}_3)$  calculated in kcal/mol at the RHF level and in parentheses at the MP2//RHF level.

Table VIII. Optimized Bond Lengths of Transition States for Olefin Insertion of  $\text{Rh}(\text{H})(\text{C}_2\text{H}_4)(\text{CO})_2(\text{Ph}_3)$  (in Å)

	Rh—H
basal	1.639 (1a-2a), 1.631 (1b-2a), 1.628 (1b-2b)
	Rh—PH <sub>3</sub>
apical	2.391 (1b-2a)
basal	2.329 (1a-2a), 2.318 (1b-2b)
	Rh—CO
acial	2.133 (1a-2a), 2.080 (1b-2b)
basal	1.882 (1a-2a), 1.904 (1b-2a), 1.942 (1b-2a) 1.922 (1b-2b)
	Rh—CH <sub>2</sub> —
basal	2.222 (1a-2a), 2.197 (1b-2a), 2.206 (1b-2b)
	C=C in Ethylene
basal	1.410 (1a-2a), 1.410 (1b-2a), 1.399 (1b-2b)

rotation, coupled with the skeletal change from "TBP" to "SP". The ethylene rotation allows the C=C axis to become parallel to the Rh—H bond to form a "four-center active site", as shown in Figure 4 for TS(1a→2a). The skeletal change is similar to that for the BPR up to its transition state. The corresponding transition states for BPR, 1a to 1g and 1b to 1f, however, do not exist, since 1g and 1f are not in equilibrium. Between the transition states and the products,  $\text{Rh}(\text{C}_2\text{H}_5)(\text{CO})_2(\text{PH}_3)$  (2), whose optimized structures are shown in Figure 4, H moves to ethylene to form the ethyl group and the apical ligand moves to the vacant coordination site that H used to occupy. The basal ethylene and the other basal ligand trans to ethylene at the transition state would become trans to each other in the square-planar products, 2. The

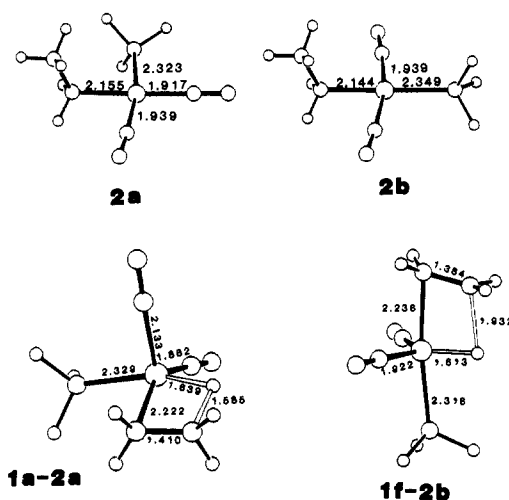
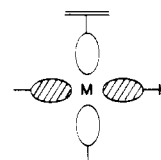


Figure 4. Optimized structures of a transition states TS(1a→2a), the product  $\text{Rh}(\text{C}_2\text{H}_5)(\text{CO})_2(\text{PH}_3)$ , and the second-order transition state 1f→2b in Å.

qualitative features of the potential energy surface leading to the olefin insertion from 1a and 1b are shown in Chart II.

The transition-state optimization starting from the structure close to 1a' with axial H and upright equatorial ethylene resulted in the ethylene dissociation to go to 3b and ethylene. The initial geometry with equatorial ethylene rotated by 45°, between 1a and 1a', also gave the same result. The upright ethylene is so unstable that dissociation supersedes the insertion. The search for the transition state from 1d led to the transition state for the BPR connecting 1d and 1f. No transition state for olefin insertion from 1d could be found. On the other hand, under the constraint of C<sub>s</sub> symmetry we have found a "transition state" for olefin insertion from 1f. The optimized structure is shown in Figure 4. However, this is not a true transition state but rather the second-order transition state with two imaginary frequencies connecting the transition state for olefin insertion from 1b to 2b and the "enantiomer" of the same transition state. This second-order transition state is higher in energy only 1 kcal/mol than the transition state for olefin insertion from 1b, and the activation barrier for olefin insertion from 1f is calculated to be only 0.5 kcal/mol. We did not search transition states from 1b with the equatorial ethylene forced upright or form 1e since they are expected to be similar to those from 1a' and 1d, respectively.

The above results show that the olefin insertion takes place only via "square-pyramidal" transition states (paths 4 and 5 in Scheme III) but via "trigonal-bipyramidal" transition states (paths 1 to 3). This difference may be explained in terms of availability of a vacant metal d orbital during the reaction. There have appeared a few studies that investigate the orbital interaction governing the olefin insertion.<sup>15,16,20,34</sup> Although the words used are slightly different, the important factor that emerges for olefin insertion is the participation of a formally vacant d orbital in the reaction. For instance, the d<sup>8</sup> four-coordinate complex, where olefin insertion takes place easily, has a vacant d orbital, say d<sub>x<sup>2</sup>-y<sup>2</sup></sub>, as shown below.<sup>20</sup>



(34) (a) Fukui, K.; Inagaki, S. *J. Am. Chem. Soc.* **1975**, *97*, 4445. (b) Steigerwald, M. L.; Goddard, W. A. *J. Am. Chem. Soc.* **1984**, *106*, 308. (c) Fujimoto, H.; Yamasaki, T.; Mizutani, H.; Koga, N. *J. Am. Chem. Soc.* **1985**, *107*, 6157.

(35) (a) Armstrong, D. R.; Perkins, P. G.; Stewart, J. J. P. *J. Chem. Soc., Dalton Trans.* **1972**, 1972. (b) Novaro, O.; Blaisten-Barojas, E.; Clementi, E.; Giunchi, G.; Ruiz-Vizcaya, M. E. *J. Chem. Phys.* **1978**, *68*, 2337. (c) Dedieu, A. *Inorg. Chem.* **1981**, *20*, 2803. (d) Backvall, J.-E.; Bjorkman, E. E.; Pettersson, L.; Siegbahn, P. *J. Am. Chem. Soc.* **1984**, *106*, 4369.

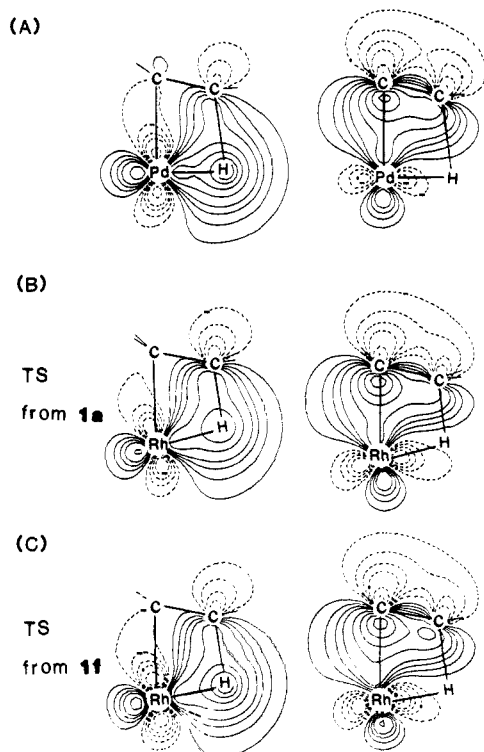
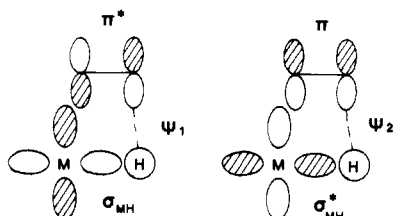
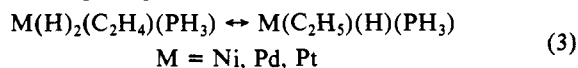


Figure 5. Boys localized molecular orbitals representing four-centered transition state of olefin insertion for  $\text{Pd}(\text{H})_2(\text{C}_2\text{H}_4)(\text{PH}_3)$ , **1a**, and **1f**.

This d orbital contributes to an M-H bond and also accepts electron from the ethylene  $\pi$  orbital. At the transition state of olefin insertion, if the d orbital is vacant, in addition to the  $\sigma_{\text{MH}} \rightarrow \text{C}=\text{C} \pi^*$  back-donative interaction, the  $\text{C}=\text{C} \pi \rightarrow \sigma_{\text{MH}}^*$  donative interaction can take place, both of which are essential for the bond exchange during the reaction.



Previously, we have studied olefin insertion/ $\beta$ -elimination of group 10  $d^8$  square-planar transition metal complexes.<sup>20</sup>



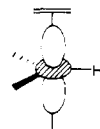
We show in Figure 5A Boys localized molecular orbitals (LMOs) that are occupied and localized in the four-center region at the transition structure of Pd. Though the LMO on the left and the right happen to represent linear combinations of LMOs,  $\psi_1 - \lambda\psi_2$  and  $\lambda\psi_1 + \psi_2$ , respectively, they demonstrate clearly the importance of both donative and back-donative interaction. Even in complexes other than  $d^8$  four-coordinate, olefin insertion would be feasible, if there is a vacant d orbital that can participate in the back-donative interaction.

In the square-pyramidal structures of the present  $d^8$  five-coordinate complex, actually the formally vacant  $d_{x^2-y^2}$  orbital is available.



Therefore, the orbital interaction at the transition state would be similar to that of the above mentioned  $d^8$  four-coordinate square-planar complex. Actually one can find two LMOs at the transition state of olefin insertion from **1a** to **2a**, as shown in Figure 5B, which are very similar to those of Pd in part A.

The LMOs shown in Figure 5C indicate that an appropriate vacant d orbital is also available at the "transition state" from **1f** with axial ethylene and equatorial H as shown below.



The olefin insertion from **1f** is orbitally acceptable. It does not actually proceed, however, because it is energetically too high due to unfavorable axial ethylene and equatorial H. The same orbital might be effective in the reaction from **1a** if ethylene is rotated to be upright. However, the upright equatorial ethylene makes the system too unstable, as was discussed, and the olefin insertion cannot take place. Thus the TBP paths (1) and (2) are not available because their energies are too high due to unfavorable ligand effects, even though a vacant d orbital for bond exchange is available.

The situation is quite different for path (3), the reaction of **1d** with equatorial H and ethylene. For olefin insertion to take place through a TBP transition state, one needs a vacant d orbital within the equatorial plane. This is not available, and thus path (3) is closed. One may note that **1d** or **1e** cannot rearrange through BPR into an SP geometry where ethylene and H are cis to each other for each other for easy insertion reaction.

In spite of the similarity in the orbital interactions, the activation barriers calculated for ethylene insertion of the present  $d^8$  five-coordinate complexes, **1a** and **1b**, are 20–21 kcal/mol, larger than that for ethylene insertion of  $d^8$  four-coordinate group 10 transition-metal complex: 8.0 kcal/mol for Pd and 12.5 kcal/mol for Pt at the RHF level of calculation.<sup>20</sup> The present barrier is similar to 18.4 kcal/mol, calculated previously for ethylene insertion of Rh  $d^6$  six-coordinate complex.<sup>23</sup> At the transition state of the present complex (cf. Figure 4), the Rh-H bond to be broken is short and close to that in the reactant and the C-H bond to be formed is still very long, indicating that the transition state is in an "early" stage of bond exchange. This suggests that the most important origin of the activation energy is not the bond exchange but the skeletal deformation required to reach the SP structure ready for olefin insertion. This skeletal deformation of **1a** and **1b** from TBP to SP is similar to that of the first half of the BPR process from **1a** to **1g** and **1b** to **1f**, respectively. Thus, the energy required for the skeletal deformation can be estimated roughly to be about 10 kcal/mol, a half of the energy difference for **1a**  $\rightarrow$  **1g**. The remainder of the barrier, about 10 kcal/mol, is ascribable to the ethylene rotation in the SP structure required to make the C=C bond parallel to the Rh-H bond. The low activation barrier of olefin insertion from **1f** is clear evidence that the change of the structure is the origin of the activation barrier and is in line with Thorn and Hoffmann's assessment.<sup>15</sup> The large change of the structure was not necessary for olefin insertion in group 10  $d^8$  four-coordinate complexes, where the barrier is much lower.

In some semiempirical and ab initio MO calculations on olefin insertion of  $d^8$  five-coordinate complexes,  $\text{Pt}(\text{H})(\text{Cl})(\text{C}_2\text{H}_4)(\text{P}-\text{H}_3)_2$ ,<sup>16</sup>  $\text{Co}(\text{H})(\text{C}_2\text{H}_4)(\text{CO})_3$ ,<sup>17</sup> and  $\text{Pd}(\text{Cl})_3(\text{H})(\text{C}_2\text{H}_4)$  dianion,<sup>18</sup> low activation barriers have been obtained under the assumption of  $C_s$  symmetry. This assumption corresponds to the process **1f**  $\rightarrow$  **2b** in Figure 3. The reactant is unrealistically unstable and the barrier is artificially low. As demonstrated in the present paper, nonsymmetric square-pyramidal structures have to be considered.

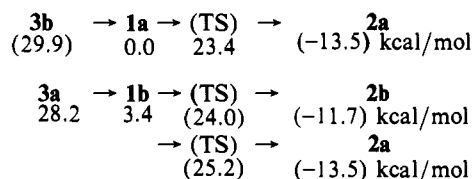
### Concluding Remarks

We have investigated the potential energy surface for the rearrangement of  $\text{Rh}(\text{H})(\text{C}_2\text{H}_4)(\text{CO})_2(\text{PH}_3)$ . The equilibrium structures of this  $d^8$  five-coordinate complex are regarded as "trigonal bipyramidal". The site preference of axial H and equatorial ethylene has been found. The "trigonal-bipyramidal" structure with equatorial H and axial ethylene is not equilibrium but the transition state connecting the most stable "trigonal-bipyramidal" structures with axial H and equatorial ethylene. The



other kind of possible structures of a five-coordinate compound, "square pyramids", is the transition state for rearrangement connecting the "trigonal-bipyramidal" equilibrium structures. The transition-state structures indicate that the rearrangement occurs via the Berry pseudorotation mechanism. The intrinsic activation barrier for Berry pseudorotation is calculated to be only a few kcal/mol. The potential energy surface for olefin coordination to Rh(H)(CO)<sub>2</sub>(PH<sub>3</sub>) has been investigated as well. As expected, the electron correlation is very important in determining this energetics. We have also determined the transition structures for intramolecular olefin insertion of Rh(H)(C<sub>2</sub>H<sub>4</sub>)(CO)<sub>2</sub>(PH<sub>3</sub>). The reaction starts from the most stable isomers of the olefin complex with axial H and equatorial ethylene and goes through an early transition state with basal H and basal ethylene in which Rh—H is parallel to the C=C bond, before reaching the square-planar ethyl complex. The activation barrier is calculated at the RHF level to be 20–21 kcal/mol. This barrier is higher than that calculated previously for group 10 complexes. The origin of the activation barrier is ascribed to the change of the skeleton to the square pyramidal.

As has been discussed in the introduction, the overall goal of the present project is to calculate the potential energy profile of the entire catalytic cycle presented in Scheme II and to provide insight into the nature and the controlling factors of the catalytic system. In the present paper, we have covered only two steps in the catalytic cycle. Combining the results for olefin coordination and rearrangement in Figure 1 and for olefin insertion in Figure 3, one can find that there are three favorable direct paths from Rh(H)(CO)<sub>2</sub>(PH<sub>3</sub>) (**3**) through Rh(H)(C<sub>2</sub>H<sub>4</sub>)(CO)<sub>2</sub>(PH<sub>3</sub>) (**1**) to Rh(C<sub>2</sub>H<sub>5</sub>)(CO)<sub>2</sub>(PH<sub>3</sub>) (**2**).



The numbers are relative energies in kcal/mol at the MP2 level, with those in parentheses representing an MP2 estimate from the RHF calculation. In all these paths, the energetics is comparable and the mechanism is similar; **3** goes with no or a small barrier to the most stable isomers of **1**, which, without any rearrangement among isomers of **1**, climb up a substantial barrier and then exothermically reach **2**. It is also possible for **3** to form **1d** or **1e**, which then have to rearrange through the BPR to isomers **1a** or **1b**, respectively, before olefin insertion can take place to yield **2**. Studies on the other steps of the catalytic cycle will continue in our laboratory.

**Acknowledgment.** The authors acknowledge Drs. R. L. Martin and P. J. Hay for providing an effective core potential subroutines. All the calculations were carried out at the Computer Center of Institute for Molecular Science.

**Registry No.** **1**, 113860-09-6; Rh(H)(CO)<sub>2</sub>(PH<sub>3</sub>), 113975-04-5.

**Supplementary Material Available:** Tables of full optimized geometrical parameters for all the equilibrium and the transition structures (12 pages). Ordering information is given on any current masthead page.

## Computational Evaluation and Comparison of Some Nitramine Properties

Peter Politzer,\* Nagamani Sukumar, Keerthi Jayasuriya, and Shoba Ranganathan

Contribution from the Department of Chemistry, University of New Orleans, New Orleans, Louisiana 70148. Received September 16, 1987

**Abstract:** A computational study of six nitramines, R<sub>1</sub>R<sub>2</sub>NNO<sub>2</sub>, has been carried out with the objective of gaining a better understanding of how the properties of the NNO<sub>2</sub> group are affected by the natures of R<sub>1</sub> and R<sub>2</sub>. An ab initio SCF procedure was used, with the initial step being the determination of each molecule's optimized geometry. This was subsequently used to compute its bond orders, dipole moment, and electrostatic potential. In most instances, the NNO<sub>2</sub> portions of the molecules are planar, due to the strong electron-withdrawing effect of the nitro group; the amino-type nitrogen can better respond to this when in a planar configuration. One consequence is that the N—NO<sub>2</sub> bonds possess some degrees of double bond character; their bond orders range from 1.36 to 1.63, with the weaker bonds corresponding to the more electron-withdrawing R<sub>1</sub> and R<sub>2</sub> groups. The strong negative electrostatic potentials normally associated with the lone pairs of amino-type nitrogens are greatly weakened or eliminated in most of these molecules; several of them show evidence of significant hyperconjugation, resulting in enhanced acidic character.

There is a considerable amount of interest in nitramines, R<sub>1</sub>R<sub>2</sub>N+NO<sub>2</sub>, as high-energy compounds.<sup>1-10</sup> For example, two

(1) Stals, J.; Barraclough, C. G.; Buchanan, A. S. *Trans. Faraday Soc.* **1969**, *65*, 904.

(2) Stals, J. *Aust. J. Chem.* **1969**, *22*, 2505 and 2515.

(3) Orloff, M. K.; Mullen, P. A.; Rauch, F. C. *J. Phys. Chem.* **1970**, *74*, 2189.

(4) Iqbal, Z.; Bulusu, S.; Autera, J. R. *J. Chem. Phys.* **1974**, *60*, 221.

(5) Doyle, R. J., Jr.; Campana, J. E. *J. Phys. Chem.* **1985**, *89*, 4251.

(6) Doyle, R. J., Jr.; Campana, J. E.; Eyley, J. R. *J. Phys. Chem.* **1985**, *89*, 5285.

(7) Oyumi, Y.; Brill, T. B.; Rheingold, A. L.; Haller, T. M. *J. Phys. Chem.* **1985**, *89*, 4317.

(8) Oyumi, Y.; Brill, T. B.; Theingold, A. L. *J. Phys. Chem.* **1985**, *89*, 4824.

of the currently most effective secondary explosives are 1,3,5-trinitro-1,3,5-triazacyclohexane (RDX, I) and 1,3,5,7-tetra-nitro-1,3,5,7-tetraazacyclooctane (HMX, II).<sup>11</sup> It is particularly important, for these and related systems, to develop greater insight into the factors that affect their stabilities toward chemical agents, heat, and shock or impact.

In order to better understand how the properties of the NNO<sub>2</sub> group are influenced by the natures of the attached R<sub>1</sub> and R<sub>2</sub>,

(9) Bulusu, S.; Weinstein, D. I.; Autera, J. R.; Velicky, R. W. *J. Phys. Chem.* **1986**, *90*, 4121.

(10) Brill, T. B.; Oyumi, Y. *J. Phys. Chem.* **1986**, *90*, 2679.

(11) Urbanski, T. *Chemistry and Technology of Explosives*; Pergamon: New York, 1984; Vol. 4, Chapter 13.